TROPICAL CYCLONE RESEARCH REPORT
TCRR **150**: 1–11 (2025)
Meteorological Institute
Ludwig Maximilians University of Munich

The axisymmetric slab boundary layer model underpinning the boundary layer control of tropical cyclones

Roger K. Smith[a1] and Michael T. Montgomery[b]
[a] *Meteorological Institute, Ludwig-Maximilians University of Munich, Germany*
[b] *Dept. of Meteorology, Naval Postgraduate School, Monterey, CA, USA*

Abstract:
The dynamics of the slab boundary layer model for an axisymmetric vortex are re-examined in the light of the continued relevance of this model as a benchmark for understanding aspects of tropical cyclone structure. Of particular relevance is the control the boundary layer has on the location of deep convection. Using two different methods to solve for the steady nonlinear boundary layer, it is shown that in relatively narrow vortices, the location of maximum ascent out of the boundary layer lies inside the radius of maximum gradient wind. In contrast, as the breadth of the gradient wind profile increases, the location of maximum ascent moves outwards beyond that of the maximum gradient wind. These new findings help to understand airborne Doppler radar observations of certain structural differences between rapidly developing and mature storms. Shown also is the propensity of the boundary layer of broad vortices to produce secondary maxima of tangential wind and ascent out of the boundary layer well beyond the radius of maximum gradient wind. This intrinsic boundary layer feature has relevance to understanding secondary eyewall formation. Some implications of the new calculations to translating vortices and to the theory of potential intensity are discussed also.

KEY WORDS Tropical cyclones, slab boundary layer, agradient force, subgradient winds, supergradient winds, shocks

Date: July 13, 2025; Revised ; Accepted

1 Introduction

As summarized in a recent paper by the authors, two key dynamical features of tropical cyclones are the frictional boundary layer and the overturning circulation associated with deep cumulus convection (Smith and Montgomery 2025b). The boundary layer is important for two reasons. Firstly, it leads to a convergence-divergence pattern that enables it to exchange fluid with the interior vortex flow. The low-level, frictionally-driven inflow is accompanied through continuity by outflow above it, which, by itself, would lead to a spin-down of the vortex by the accompanying outward flux of absolute vorticity. Secondly, the boundary layer is important for its ability to supply the vortex core with moisture enriched air to maintain the inner-core deep convection required for the intensification of these storms.

For a tropical cyclone to intensify, deep convection is necessary in the inner vortex core to drive an overturning circulation with inflow in the lower troposphere and outflow above, the inflow branch being strong enough to oppose the persistent outflow that would otherwise be produced by the boundary layer. Surface moisture fluxes from the ocean are required to elevate the equivalent potential temperature of the boundary layer air in the core of the vortex. This moisture elevation serves to maintain deep convection and thereby a persisting inflow above the boundary layer to more than compensate the boundary layer induced outflow.

Except in the immediate neighborhood of the convection, the rate at which mass converges in the boundary layer is controlled by the tangential wind profile at the top of the boundary layer, while the mass flux carried aloft by convection depends, inter alia, on the thermodynamic properties of air ascending into the convection. There is no physical reason to expect that at all times during the tropical cyclone life cycle, the mass converging in the boundary layer will be exactly equal to that being ventilated vertically by deep convection.

In summary, the most important factor governing tropical cyclone intensification is the ability of inner-core deep convection to ventilate moist air at a rate larger than that converging in the boundary layer and to carry this air to the upper troposphere. Under these circumstances, the convection will drive inflow above the boundary layer, which is necessary to concentrate absolute vorticity required to intensify the vortex (Kilroy et al. 2016; Smith et al. 2021a; Smith and Montgomery 2025b). This framework has been adopted successfully in a recent observational study aimed at understanding the relationship between the azimuthally averaged kinematic structure of the tropical cyclone boundary layer and storm intensity, intensity change, and vortex structure above the boundary layer (Zhang et al. 2023).

[1]Correspondence to: Prof. Roger K. Smith, Meteorological Institute, Ludwig-Maximilians University of Munich, Theresienstr. 37, 80333 Munich. E-mail: roger.smith@lmu.de

As discussed in Smith and Montgomery (2025a), classical boundary layer theory follows a standard pattern. A scale analysis for a thin layer with friction demonstrates that, to a good first approximation, the stress terms in the governing Navier-Stokes equations can be approximated by those normal to the boundary and that the pressure gradient parallel to the boundary is equal to that in the inviscid flow above the boundary layer. For the large Reynolds numbers that typically characterize tropical cyclone vortices, the flow above the boundary layer satisfies Euler's equations of motion at leading order. The foregoing approximation associated with the boundary layer flow enables the pressure gradient within the layer to be prescribed in terms of the flow exterior to the layer when that flow is known. Vortex boundary layers normal to the axis of rotation do have a special property compared, for example, with those in simple aerodynamic flows, because of their ability to expel boundary layer fluid into the exterior flow, or to draw exterior fluid into the layer. Strictly speaking, this means that the exterior flow cannot be formulated independently of the boundary layer flow, except with further assumptions. In general, the boundary layer and exterior flows have to be solved together.

As discussed in Smith and Montgomery (2025a) also, theories for the tropical cyclone boundary layer have fallen into two types: those that take into account the vertical structure of the boundary layer, itself, and those that treat the boundary layer as a slab with uniform properties. The former suffer from the limitation of requiring that any flow expelled from the boundary layer returns immediately to the prescribed exterior flow as it exits the layer (Smith and Montgomery 2010).

While analyzing the axisymmetric boundary layer solutions as control for interpreting those for a translating vortex in Smith and Montgomery (2025a), we noticed certain properties that appeared to offer explanations of some observed characteristics of tropical cyclones. These include the finding of Rogers et al. (2013) that the maximum updraught in intensifying storms lies inside the radius of maximum tangential wind while it lies outside this radius in mature storms. They include also the findings of Zhang et al. (2023), who explored the idea that the explanation lies in the boundary layer and its coupling to the interior flow.

Moreover, we noticed that, as model vortices become broader, the boundary layer begins to develop a secondary maximum of tangential and vertical velocity substantively beyond the radius of maximum gradient wind, As the broadening continues, the outer maxima exceed the inner ones. These features would seem relevant to understanding secondary eyewall formation as suggested by Abarca and Montgomery (2013).

The primary motivation of the present paper is to explore the foregoing connections further without the added complication of vortex translation.

2 The slab boundary layer model

The calculations presented here are based, in part, on a one-dimensional version of the simplified slab boundary layer formulation employed by the authors in a recent paper studying the effects of vortex translation on boundary layer flow asymmetries (Smith and Montgomery 2025a). The principal simplifications involve using a constant depth for the boundary layer, a constant drag coefficient and the neglect of the downward transport of momentum through the top of the boundary layer, which was shown by Smith and Vogl (2008) to have only a small effect on their slightly more complete solutions, and finally the neglect of vortex translation. These simplifications are in the spirit of the insightful recognition by James (1994) that "comprehensive complexity in modelling is not a virtue, but rather an admission of failure".

In a cylindrical coordinate system and with the boundary layer density assumed constant, the steady, vertically-integrated equations for the radial momentum, azimuthal momentum and mass continuity can be written in the following form:

$$u_b\frac{du_b}{dr} = -\frac{(v_g^2 - v_b^2)}{r} - f(v_g - v_b) - \frac{C_D}{h}(u_b^2 + v_b^2)^{\frac{1}{2}}u_b, \tag{1}$$

$$u_b\frac{dv_b}{dr} = -\left(\frac{v_b}{r} + f\right)u_b - \frac{C_D}{h}(u_b^2 + v_b^2)^{\frac{1}{2}}v_b, \tag{2}$$

$$\frac{du_b}{dr} = -\frac{u_b}{r} - \frac{w_h}{h}, \tag{3}$$

where u_b and v_b are the vertically-averaged radial and azimuthal components of velocity in the boundary layer, $v_g(r)$ and w_h are the gradient wind and vertical velocity at the top of the boundary layer, f is the Coriolis parameter, and C_D is the surface drag coefficient. The quantities u_b and v_b are assumed to be independent of depth. As in Smith and Montgomery (2025a), we take $C_D = 2.0 \times 10^{-3}$.

Smith and Montgomery (2008) showed that at radii large enough for the radial flow to be small compared with the gradient wind and for the nonlinear terms in Eqs. (1) and (2) to be neglected, the equations can be linearized with respect to the gradient wind and solved to give

$$u_b = -\mu v_g, \tag{4}$$

and

$$v_b = v_g(1 - \nu^2), \tag{5}$$

where

$$\mu = \frac{C_D v_g}{h\zeta_{ag}}. \tag{6}$$

and

$$\nu = \frac{C_D v_g}{hI_g}, \tag{7}$$

where ζ_{ag} is the absolute vorticity of the gradient wind, $I_g^2 = \xi_g\zeta_{ag}$ is the inertial stability parameter and $\xi_g =$

$2v_g/r + f$ is twice the absolute angular rotation rate of the gradient wind. These solutions, which are valid only if the characteristic Ekman numbers μ and ν are small compared with unity, are the slab equivalent of the generalized Ekman layer (cf. Smith and Montgomery (2023), Chapter 6). An assessment of the self-consistency of this linearized Ekman-type solution for a hurricane-strength vortex is provided below as part of the interpretation of the nonlinear boundary layer solutions.

2.1 Prescribed gradient wind profiles

The prescribed vortical flow above the boundary layer, $v_g(r)$, is taken to be axisymmetric and in gradient wind balance. Here we choose a range of simple tangential wind profiles

$$v_g(r) = \frac{v_o s}{1 + s^x}, \tag{8}$$

where $v_o = 2v_{max}$, $s = s_{max} r/r_{max}$, α is a dimensionless constant and $s_{max} = [1/(x-1)]^{1/x}$ to ensure that $dv_g/dr = 0$ when $r = r_{max}$. Choosing this value for s_{max} makes $r = r_{max}$ when $s = s_{max}$. Six profiles are examined with x ranging from 1.3 to 2.3 in steps of 0.2 (Fig. 1). For the same values of $v_{max} = 45$ and r_{max}, the breadth of the outer profile of v_{gr} increases as the parameter x decreases. Choosing values $v_{max} = 45$ m s^{-1} and $r_{max} = 40$ km, these vortices are inertially (centrifugally) stable (i.e., $I_g^2 > 0$) for a Coriolis parameter $f = 5 \times 10^{-5}$ s^{-1} that corresponds with a latitude of approximately 20^{o}N.

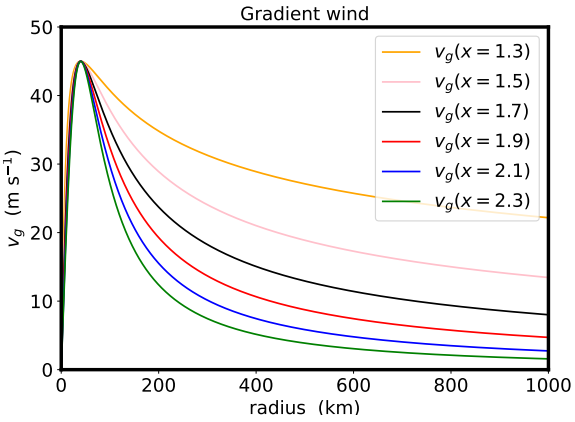

Figure 1. Radial profiles of gradient wind for the six values of x used in the calculations.

2.2 Solution methods

We employed two methods of solving the steady nonlinear equations (1) and (2). The first method, designated Method 1, adds time derivative and lateral diffusion terms and integrates these equations to a steady state as in Smith and Montgomery (2025a). The method employs a regular grid in radius with 1 km grid spacing over a domain of radius 1000 km. Both u_b and v_b were taken to be zero at the axis and open boundary conditions were imposed on these velocities at the domain boundaries requiring normal velocities to have zero gradient there. Second-order centred differencing was used and the gradient wind v_g with zero radial flow, $u_b = 0$, was used as the initial condition in all cases. The versions of Eqs. (1) and (2) with time derivatives and diffusion terms added were advanced in time using a third-order Runge-Kutta scheme until the velocities had attained a steady state, which, typically requires about 20,000 time steps. The time step, Δt, was normally 10 seconds, but was halved if the Courant-Friedrichs-Lewy (CFL) parameter, $V_{max}\Delta t/\Delta r$, exceeded 0.3, where V_{max} is the maximum *total* horizontal wind speed and Δr is the radial grid spacing.

The second method, designated Method 2, is to integrate the equations equations inwards from the outer boundary taking the linear solution, Eqs. (4) and (5), as starting values. Again, a third-order Runge-Kutta scheme was used with a radial grid of 1 km and the radial boundary at 1000 km. No horizontal diffusion was required using this method and the method is asymptotically in accord with the boundary layer equations for a slab layer.

Finally, the linear solution was calculated as a function of radius from Eqs. (4) and (5) for comparison with Methods 1 and 2.

3 Solutions

Figure 2 shows the radial profiles of the steady-state radial and tangential velocity components in the boundary layer for the two nonlinear methods of calculation and for the linear solution together with the gradient wind at the top of the boundary layer for the six gradient wind profiles in Fig. 1. In this figure, the radial velocity is plotted with positive values representing inflow and negative values representing outflow.

Some notable features of the solutions are as follows:

- On the domain shown, there is almost perfect agreement between the two methods of solving the nonlinear equations, at least before the radial flow in the boundary layer becomes zero, in which case Method 2 becomes singular and the integration must be terminated. In contrast, on account of the lateral diffusion, Method 1 captures the behaviour of the velocity components inside this radius;
- At large radii the maximum tangential velocity in the boundary layer is less than the gradient wind, (i.e., subgradient), but in the nonlinear solutions, it exceeds the gradient wind (i.e., supergradient) at some inner radius;
- The radius at which the tangential wind first becomes supergradient as the radius decreases becomes larger as the gradient wind profile broadens;

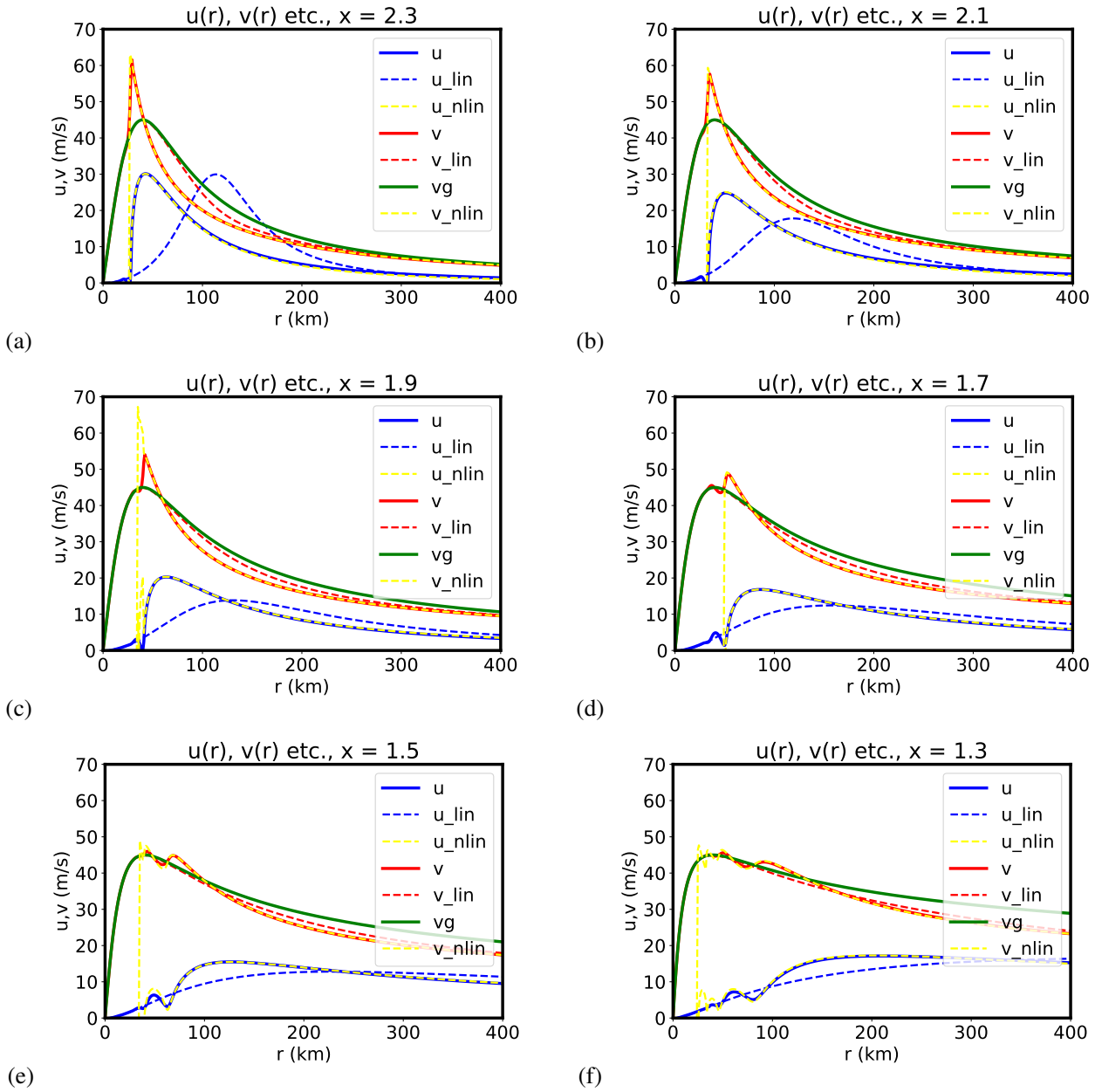

Figure 2. Radial profiles of gradient wind, v_g, together with those of radial and tangential velocity components in the boundary layer calculated using the two nonlinear methods of solution and the corresponding linear solution (red dashed curves) for the six values of the profile parameter, x: (a) 2.3, (b) 2.1, (c) 1.9, (d) 1.7, (e) 1.5 and (e) 1.3. In each panel, the radial velocity is plotted with positive values representing inflow and negative values outflow. In the legend of each panel, u and v refer to tangential and radial velocity components of the nonlinear solution obtained by Method 1, u_nlin and v_nlin refer to those obtained by Method 2 and u_lin, v_lin refer to the linear solution.

- There is a rapid deceleration of the radial inflow at radii where v_b exceeds v_g, since, at these radii, all the forces in the radial direction are directed outwards;
- For the relatively narrow vortex profiles ($x = 2.3$ and $x = 2.1$), the nonlinear solution(s) for the tangential velocity in the boundary layer significantly exceed that of the gradient wind at the top of the boundary layer. The tangential wind maximum occurs inside the gradient wind maximum in these cases. The wind maximum declines rapidly as the radius decreases inwards of the maximum.
- The radial wind for the profiles $x = 2.3$ and $x = 2.1$ exhibits a rapid decline just inside the tangential wind maximum also. For these cases of a narrow vortex, both the tangential and radial wind profiles near the maximum supergradient wind exhibit spatial structure akin to a shock in gas dynamics or hydraulics (e.g., Slocum et al. 2014).
- The linear solution is an acceptable approximation

to the nonlinear solutions at large radii, except possibly for the broadest gradient wind profiles ($x = 1.3$ and $x = 1.5$), but tends to overestimate both the tangential and radial velocity components obtained in the nonlinear solutions at these radii. In particular, at a radius of 1000 km, it produces a maximum radial inflow that is somewhat larger, especially for $x = 1.3$, than the corresponding nonlinear solutions (see Fig. 6 below).

- The tangential velocity component obtained in the linear solution remains subgradient at all radii consistent with Eq. (5) when $\nu << 1$.

Of particular interest here are the differences in behaviour as the gradient wind profile broadens. These are highlighted in Fig. 3, which compares radial profiles of the radial and tangential velocity components in the boundary layer and the vertical velocity at the top of the boundary layer at radii inside 150 km for the nonlinear solutions obtained using Method 1 for the six gradient wind profiles in Fig. 1. The immediate features one notices are:

- The maximum radial inflow increases in magnitude and decreases in radius as the gradient wind profile narrows;
- The peak in tangential velocity lies inside the radius of maximum gradient wind, r_{max}, for the narrowest gradient wind profiles ($x = 2.3$ and $x = 2.1$), but moves outwards in radius, beyond r_{max}, and decreases in magnitude as the gradient wind profile broadens;
- The maximum vertical velocity has a similar behaviour to the tangential velocity, lying inside r_{max}, for the two narrowest gradient wind profiles, but moving outwards beyond r_{max} while decreasing in magnitude as the gradient wind profile broadens;
- More subtly, both the tangential and vertical velocity develop secondary maxima in the two broadest gradient wind profiles, with both the inner and outer maxima moving outwards and the outer maximum increasing in magnitude relative to the inner one as the gradient wind profile broadens.

3.1 Varying inner core radius

Observations as well as numerical modelling studies show that as tropical cyclones mature, their inner core radius grows in size as well as their outer circulation. A well documented observational case is that of Hurricane Isabel (2003) (Bell and Montgomery 2008) and a pertinent modelling study is that of Smith et al. (2021b). It follows that our investigation of the dependence of inner-core boundary layer structure on the size of the outer circulation would be incomplete without some investigation of the dependence of boundary layer dynamics on changes of the inner core radius characterized by r_{max}. For this reason, we examine the robustness of the results shown above, based on calculations with the same inner core radius, as the inner core radius is varied while keeping the gradient wind breadth parameter x the same. To this end, we show in Fig. 4 boundary layer calculations using Method 1 for the narrowest gradient wind profile with $x = 2.3$ and a broader profile with $x = 1.9$ for values of r_{max} of 20 km and 30 km, compared with the calculations for $r_{max} = 40$ km discussed earlier in this section.

In the narrowest vortex case ($x = 2.3$), the previous results that the maximum tangential wind speed in the boundary layer and the maximum vertical velocity ascending out of the boundary layer, w_{max}, lie inside the radius r_{max} hold also in the case when r_{max} is reduced to 30 km and further to 20 km. The maximum tangential wind speed in the boundary layer remains more or less the same as r_{max} is reduced, but there is a reduction of the agradient wind at radii beyond r_{max}, whereby, as explained in the next section, the boundary layer inflow is reduced also. Despite the reduction of inflow, w_{max} increases as r_{max} is reduced, presumably a geometrical consequence of mass continuity.

In the broader vortex case ($x = 1.9$), the earlier results that the maximum tangential wind speed in the boundary layer and the location of w_{max} lie outside the radius r_{max} hold also in the case when r_{max} is reduced to 30 km and further to 20 km. In this case, however, the maximum tangential wind speed in the boundary layer decreases as r_{max} is reduced and, again, there is a reduction of the agradient wind at radii beyond r_{max} leading to a reduced boundary layer inflow. In this case, w_{max} decreases as r_{max} is reduced.

In the next section, we provide interpretations for much of the foregoing behaviour and discuss the relevance of the slab boundary layer calculations for understanding a range of tropical cyclone observations.

4 Interpretations and relevance

4.1 Inner-core convective structure

The finding that the vertical velocity at the top of the boundary layer moves outwards as the gradient wind profile broadens offers an understanding for some of the composite analyses of airborne Doppler radar observations presented by Rogers et al. (2013) and Zhang et al. (2023). As summarized succinctly in Rogers et al.'s Fig. 16, intensifying tropical cyclones have a ringlike vorticity structure inside the radius of maximum wind; lower vorticity in the outer core; a deeper, stronger inflow layer; and stronger axisymmetric eyewall upward motion compared with mature tropical cyclones. Invoking Stokes' theorem, lower vorticity in the outer core is synonymous with a narrower outer circulation or, in our parlance, a narrower gradient wind profile.

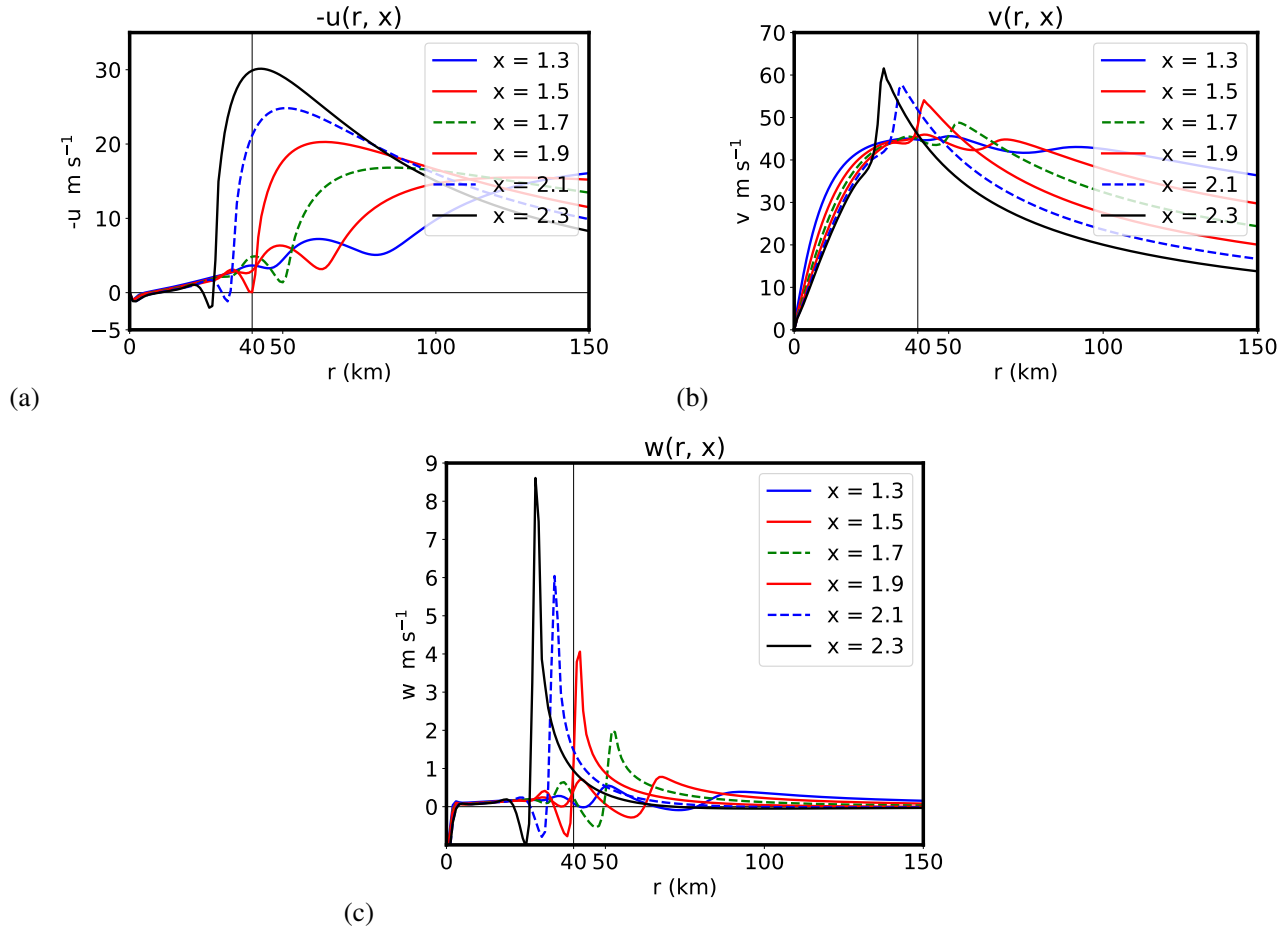

Figure 3. Radial profiles of tangential velocity components in the boundary layer and vertical velocity at the top of the boundary layer at radii inside 150 km in the nonlinear solutions obtained using Method 1 for the six gradient wind profiles in Fig. 1. The radial velocities in (a) are plotted with positive values representing inflow and negative values outflow. The location of the radius of maximum gradient wind at 40 km is highlighted in each panel by a thin vertical line.

Observations, supported by numerical modelling studies show that the tangential wind field of storms has a natural tendency to broaden during the storm's life cycle (e.g., Sampson et al. 2017, Smith et al. 2021b). The tendency of the outer circulation to grow in size may be understood in terms of the fact that, at radii where the convectively-driven overturning circulation is strong and persistent enough to draw air inwards above the boundary layer, absolute vorticity will be drawn inwards to increase the circulation at that radius.

Our simple slab boundary layer solutions suggest that the location of the eyewall convection is strongly controlled by the boundary layer dynamics, with narrower vortices having a stronger updraught ascending from the boundary layer inside the radius of maximum gradient wind, while in broader vortices, the location of maximum ascent out of the boundary layer moves outside this radius. Since the roots of deep convection originate in the boundary layer, it seems reasonable to invoke the principle of boundary layer control in determining the location of deep convection, despite the fact that, as explained earlier, it is not a given that all the air that ascends out of the boundary at any given time can be ventilated by deep convection triggered by the ascent, itself.

The question remains as to *why* the maximum ascent out of the boundary layer moves outwards as the gradient wind profile broadens. A notable feature of the solutions shown in Fig. 2 is the increasing reduction of the local tangential wind in the boundary layer at outer radii compared with the gradient wind as the gradient wind profile becomes broader. This reduction implies a larger inward agradient force per unit mass given by

$$agf = \frac{v^2 - v_g^2}{r} + f(v - v_g). \tag{9}$$

A summary of this difference is highlighted in Fig. 5, which compares profiles of the agradient force at radii greater than 200 km for the six profiles of gradient wind shown in Fig. 1. The principal curves are based on the nonlinear boundary layer calculations using Method 1 (thick curves), but the corresponding curves for the linear solution are shown also (thin curves). The corresponding

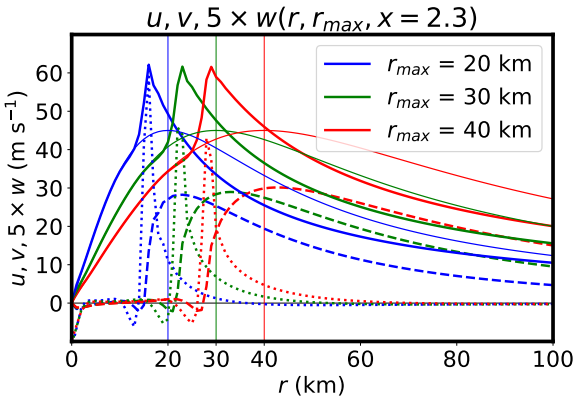

(a)

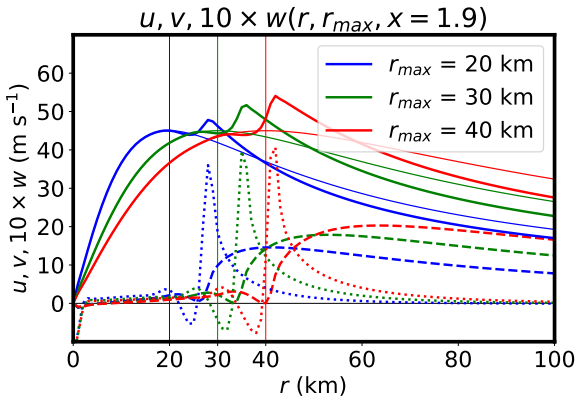

(b)

Figure 4. Radial profiles of the boundary layer radial (dashed curves) and tangential (solid curves) velocity components u, v, a scaled vertical velocity w at the boundary layer top (dotted curves) and the gradient wind, v_g, (thin red curves) in the nonlinear solutions obtained using Method 1 with gradient wind profiles with (a) $x = 2.3$ and (b) $x = 1, 9$ with three different radii of maximum gradient wind r_{max} indicated by the three vertical lines.

agradient force per unit mass for the linear approximation is

$$agf_L = \left(\frac{2v_g}{r} + f\right)(v - v_g). \qquad (10)$$

Inside a certain radius that varies with the gradient wind profile parameter, x, the nonlinear calculations show an increase in the inward agradient force as the radius decreases compared with the linear solution. The relatively poor agreement of the linear and nonlinear solutions near the outer radius in the case $x = 1.3$ is simply a reflection of the fact that the conditions for the validity of the linear approximation are violated in this case. Specifically, the Rossby number based on the gradient wind at this radius is not small compared with unity and the square of the radial velocity is not small compared with the corresponding square of tangential velocity (see the Appendix).

Irrespective of the breadth of the gradient wind profile, the larger inward agradient force in the nonlinear solution drives a stronger boundary layer inflow than in the linear solution. This stronger inflow provides conditions conducive for *the boundary layer spin-up enhancement mechanism* to operate (e.g., Smith and Montgomery 2023, Section 6.6). In essence, at some outer radius, air parcels begin spiralling inwards in the boundary layer at a rate where the tangential drag on the parcel is unable to prevent the tangential wind in the boundary layer from increasing relative to the local gradient wind and eventually exceeding it at some radius.

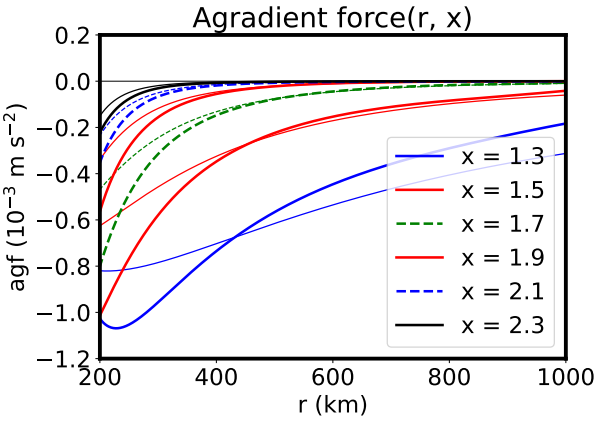

Figure 5. Radial profiles of the agradient force per unit mass, agf, in the nonlinear solutions obtained using Method 1 compared with those for the linear solution, agf_L, for the six gradient wind profiles in Fig. 1.

Note that, although the strength of the tangential drag increases as the square of the tangential velocity in the boundary layer increases, the cumulative drag decreases as the number of air parcel revolutions about the vortex axis per unit inward displacement decreases, i.e., as the radial inflow increases. One has to do the nonlinear calculation to determine at what radius the tangential velocity in the boundary layer begins to increase relative to the gradient wind and the outer radius at which it first becomes supergradient. Of course, the rate of increase of the local gradient wind with decreasing radius will be a factor also in determining this outer radius.

The calculations in Fig. 2 show that the outer radius at which the tangential flow becomes supergradient increases as the gradient wind profile broadens. When it does so, the agradient force becomes positive and leads to a rapid deceleration of the radial flow in the boundary layer. This rapid deceleration leads through continuity to a large upwards expulsion of air from the boundary layer.

Figure 3a shows that at a radius of 150 km, the radial inflow increases as the gradient wind profile broadens, a behaviour which is apparent also in Fig. 2 out to 400 km. Invoking the discussion of the previous paragraph, the larger radial inflow in the broader profiles would

suggest why the boundary layer flow might[1] become supergradient at a larger radius as the gradient wind profile broadens. Since the same profile dependence of radial inflow is found all the way out to 1000 km, where, in all except perhaps the two broadest gradient wind profiles ($x = 1.3$ and $x = 1.5$), the linear solution serves as a good approximation to the nonlinear solution, the reason for the dependence can be reasonably sought in the linear solution. Like the nonlinear solution, the linear solution does, in fact show a significant increase in inflow at the radial boundary as the parameter x decreases (Fig. 6).

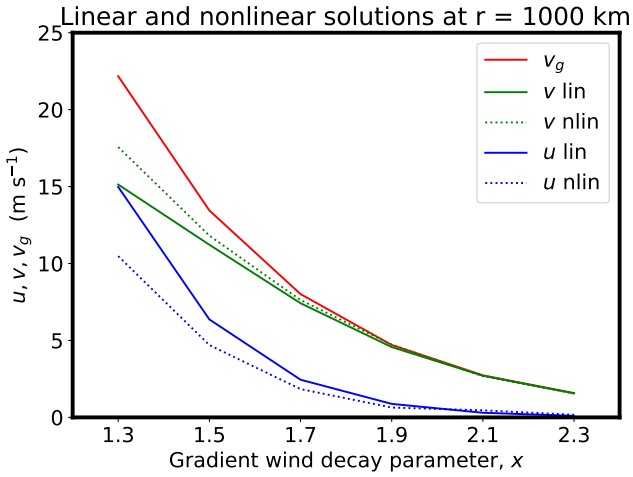

Figure 6. Variation of the gradient wind, v_g, tangential velocity v and radial velocity u at the outer boundary in the linear and nonlinear solutions (designated "lin" and "nlin", respectively) at the outer radial boundary (r = 1000 km) for the six gradient wind profiles in Fig. 1. The radial velocity is plotted with positive values representing inflow.

A little inside a radius of 150 km, the behaviour of the radial inflow on the parameter x reverses and subgradient flow is maintained until increasingly smaller radii by the rapidly increasing gradient wind as the radius decreases, an effect highlighted in the upper panels of Fig. 3. Another feature of note is the increase in the maximum agradient wind as the gradient wind profile becomes narrower. This feature can be best understood in terms of an alternative explanation for the boundary layer spin-up enhancement mechanism articulated by Montgomery and Smith (2017). These authors note that, as air parcels converge in the boundary layer, they lose absolute angular momentum, M, to the surface. Now, recall that the tangential velocity v is related to M by solving the formula defining M to give

$$v = \frac{M}{r} - \frac{1}{2}fr. \qquad (11)$$

[1]The word "might" here is required, acknowledging that one has to do the nonlinear calculation to be sure.

From this expression we see that if the rate of loss of M is sufficiently small (i.e., less than the rate of decrease of the radius of the air parcel), the corresponding tangential velocity given by Eq. (11) may increase so that, at some inner radius, the tangential wind speed in the boundary layer becomes supergradient. It is clear from Eq. (11) that the boundary layer spin-up enhancement mechanism will be more effective if the rate of loss of M becomes sufficiently small at small radii. This explains why the maximum agradient wind increases rapidly as the gradient wind profile becomes narrower.

The subtle changes in inner-core behaviour when the radius of maximum gradient wind is varied while keeping the profile parameter x the same are presumably associated, in part, with small changes in the radial gradient of the gradient wind beyond its maximum. These are seen in Fig. 4 to have an impact on the magnitude of the agradient wind and thereby, from the discussion above, would affect the boundary layer inflow via changes in the accompanying inward agradient force.

4.2 Secondary eyewall initiation

These new nonlinear boundary layer calculations show that, as model vortices become broader, the boundary layer begins to develop a secondary maximum of tangential and vertical velocity substantively beyond the radius of maximum gradient wind (Figs. 2e,f, 3b,c; Fig. 7). An expanding gradient wind field has been proposed as a necessary first stage of an intrinsic pathway for secondary eyewall formation (Abarca and Montgomery 2013, 2014; Abarca et al. 2015, 2016; Huang et al. 2012, 2018). The basic idea is that an expanding swirling flow is conducive to the generation of a radial zone of supergradient winds and related boundary layer convergence outside of the primary eyewall.

The present calculations support the foregoing pathway by showing directly that the strengthened boundary layer inflow in the outer region, which accompanies the expanding gradient wind field, serves to activate the boundary layer spin-up enhancement mechanism prior to air parcels arriving at the radius of maximum gradient wind. With the boundary layer spin-up mechanism so activated, the tangential winds exceed that of the gradient wind at the boundary layer top and all of the forces in the radial momentum equation become directed outwards. The inflowing air parcels are then rapidly decelerated. The radial deceleration leads to a zone of convergence in the boundary layer and thereby to reduced convective inhibition in the ascending air.

If the thermodynamic conditions in this region are favourable to support deep convective activity, and if the horizontal straining of convective elements is limited by the reduction of the radial shearing that accompanies the development of a local maximum in supergradient wind, the convergence zone would serve to initiate sustained deep convective activity in the supergradient wind zone.

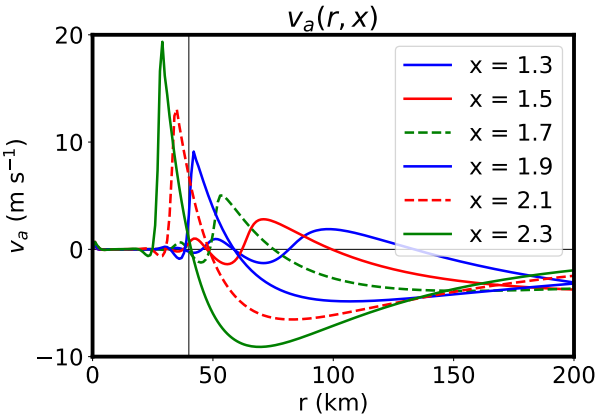

Figure 7. Radial profiles of the agradient wind, v_a, in the nonlinear solutions obtained using Method 1 for the six gradient wind profiles in Fig. 1.

In summary, these calculations help support and clarify the boundary layer control hypothesis of secondary eyewall formation.

4.3 Application to translating vortices

An important finding of tropical cyclone intensification in a translating storm by Persing et al. (2025) is that, because of flow asymmetries which emerge from the translation, intensification by the classical mechanism (i.e., a convectively-induced influx of cyclonic absolute vorticity above the boundary layer) may take place only in a restricted range of azimuths in sectors where deep convection is most active. Persing et al. found that in this case "storm-relative tangential velocity is amplified in the main updraught sector by the strong inward flux of absolute vorticity in the lower troposphere there. This vorticity is subsequently transported into the remaining sectors by the tangential circulation, where there is a weak outward vorticity flux that alone would lead to spin down." With this finding in mind, the present results should apply with some modification to translating storms as well.

4.4 Application to potential intensity theory

The foregoing slab boundary layer calculations are novel and point to the important role of the outer wind structure in determining the maximum system-scale tangential and radial wind of the boundary layer. For relatively narrow outer wind profiles, the results demonstrate that the tangential winds can significantly exceed the gradient wind maximum and this maximum can occur well inside the radius of maximum gradient wind. Both of these features have been confirmed observationally using high-resolution dropwindsonde deployments in conjunction with aircraft reconnaissance data and airborne dual-Doppler radar analyses for intensifying tropical cyclones (Montgomery et al. 2014, Sanger et al. 2014).

In the context of potential intensity theory and its extension to account for unbalanced effects at and above the boundary layer top by Bryan and Rotunno (2009), the present calculations offer an opportunity to quantitatively assess a conjecture made by them in subsequent research in regards to the practical usefulness of the Emanuel (1986) (hereafter E86) model that underpins the theory for the maximum gradient wind intensity of tropical cyclones. In the E86 formulation (and subsequent variants - see Smith and Montgomery 2023, Chapter 13, for a detailed summary), a simplified formulation of the linearized slab boundary layer (see Section 2) is employed that uses just the tangential component of the slab Ekman layer, assumes the tangential velocity in the boundary layer *is equal to* the gradient wind at leading order, and neglects the lateral diffusion of absolute angular momentum.

On page 2296 of Rotunno and Bryan (2012), they conjectured that for practical purposes the E86 slab boundary layer model should serve as an adequate boundary layer closure for the maximum intensity problem, in part because the E86 slab model represents a compromise between offsetting effects involving nonlinear advective dynamics and the radial diffusion of horizontal momentum in the boundary layer. However, in the nonlinear boundary calculations presented above, the solution of the equations with lateral diffusion retained *is not* significantly weakened by lateral diffusion. This fact is important since the lateral diffusion employed in the calculations with vortex decay exponents 2.3 and 2.1 is 5,000 m^2 s^{-1}, notably larger than the average observed horizontal diffusivity in hurricanes possessing maximum wind speeds in the range of 40 to 60 m s^{-1} (Zhang and Montgomery 2012, their Fig. 6). The current calculations offer a quantitative rebuttal to the conjecture, at least within the context of the slab boundary layer, that horizontal diffusion will act to significantly ameliorate the concentration of momentum and entropy in the boundary layer and the lofted values thereto in the vortex interior.

The reasoning behind our rebuttal is that, despite the presence of surface drag, the strong radial inflow in the boundary layer, driven by the nonlinear agradient force, acts efficiently to concentrate absolute angular momentum in the boundary layer. As we have seen, for narrow vortex profiles, this concentration has a propensity to produce shock-like structures inside the gradient wind maximum, not unlike the shock-like structure observed in the low-level wind structure of Hurricane Hugo (Marks et al. 2008). Horizontal diffusion would have to take on unrealistically large values to ameliorate this shock structure. The results herein indicate that, unlike the potential intensity theory of E86 (and variants) with its limiting slab

boundary layer approximation, the dependence of the tangential and radial wind maxima on the structure of the outer profile is an intrinsic property of tropical cyclones.

5 Conclusions

We have re-examined the dynamics of the slab boundary layer model for an axisymmetric vortex, which, as shown, is useful as a benchmark for understanding aspects of the structure of tropical cyclones. For the first time, two different methods for solving the steady nonlinear boundary layer equations were compared: one in which the unsteady form of the equations was integrated to a steady state (Method 1) and the other in which the steady equations were integrated radially inwards from the outer boundary using the linear solution to provide the outer boundary condition (Method 2). Method 2 requires that the radial velocity remains non-zero during the integration inwards, whereas Method 1 has the advantage of providing a solution close to the rotation axis, although it requires a degree of horizontal diffusion to be included to keep the integration stable. Despite these differences, the two methods showed excellent agreement in most of the solution domain.

Solutions were shown for a range of gradient wind profiles with the same maximum wind, the same radius at which this maximum occurs, but with varying outer breadths. It was found that, in vortices whose outer circulation is relatively narrow, the location of maximum ascent out of the boundary layer lies inside the radius of maximum gradient wind. In contrast, when the outer circulation is relatively broad, the maximum ascent lies outside this radius. These findings are consistent with observations of rapidly intensifying storms in the former case and mature or slowly decaying storms in the latter case.

Shown also is the propensity of the boundary layer of broad vortices to produce a secondary tangential wind maximum well beyond the radius of maximum gradient wind, an intrinsic feature of broadening storms that we believe is relevant to understanding secondary eyewall formation. Some implications of the new calculations to translating vortices and to the theory of potential intensity were discussed also.

Appendix: Validity of the linear boundary layer solution

As shown by Smith and Montgomery (2008) in Sections 3.1 and 3.2, a necessary condition for the validity of the linear boundary layer solution, given here by Eqs. (4) and (5), is that the local Rossby number for the gradient wind, defined as $Ro_v = v_g/(r\zeta_{ag})$, where ζ_{ag} is the absolute vorticity of the gradient wind, v_g, satisfies the condition $Ro << 1$. A further requirement is that the boundary layer velocity is such that $|v_a/v_g| << 1$, where v_a is the agradient velocity in the boundary layer. Radial profiles of Ro_v for the vortex profiles in Fig. 1 are shown in Fig. 8 for the entire domain of the calculations used here, 1000 km. One may judge from this figure that the linear approximation should be a reasonable one near this boundary for all except the two broadest vortices, but that it is generally strongly violated for all gradient wind profiles at radii less than about 300 km. It is within this region that the boundary layer spin-up enhancement mechanism is operative as shown Section 4.1.

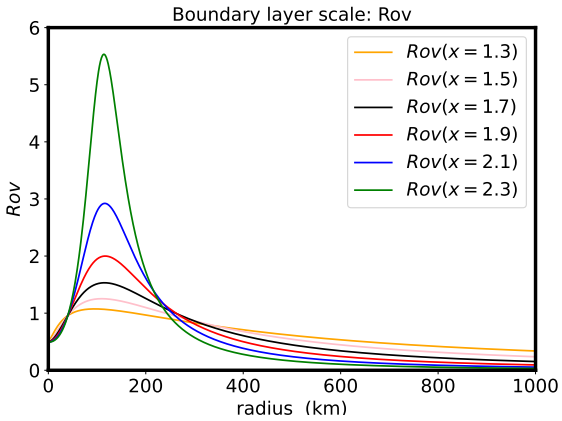

Figure 8. Radial profiles of the local Rossby number, $Ro_v = v_g/(r\zeta_{ag})$, based on the gradient wind profiles shown in Fig. 1. Here ζ_{ag} is the absolute vorticity of the gradient wind, v_g. The condition $Ro_v << 1$ is a necessary requirement that the linear boundary layer solution be valid. The nonlinear boundary layer spin-up enhancement mechanism is operative when this condition is violated.

References

Abarca, S. F., and M. T. Montgomery, 2013: Essential dynamics of secondary eyewall formation. *J. Atmos. Sci.*, **70**, 3216–3420.

Abarca, S. F., and M. T. Montgomery, 2014: Departures from axisymmetric balance dynamics during secondary eyewall formation. *J. Atmos. Sci.*, **71**, 3723–3738.

Abarca, S. F., M. T. Montgomery, S. A. Braun, and J. Dunion, 2016: On the secondary eyewall formation of Hurricane Edoard (2014). *Mon. Wea. Rev.*, **144**, 3321–3331.

Abarca, S. F., M. T. Montgomery, and J. C. McWilliams, 2015: The azimuthally-averaged boundary layer structure of a numerically simulated major hurricane. *J. Adv. Model. Earth Syst.*, **07**, 10.1002/.

Bell, M. M., and M. T. Montgomery, 2008: Observed structure, evolution, and potential intensity of Category 5 Hurricane Isabel (2003) from 12 to 14 September. *Mon. Wea. Rev.*, **136**, 2023–2046.

Bryan, G. H., and R. Rotunno, 2009: Evaluation of an analytical model for the maximum intensity of tropical cyclones. *J. Atmos. Sci.*, **66**, 3042–3060.

Emanuel, K. A., 1986: An air-sea interaction theory for tropical cyclones. Part I: Steady state maintenance. *J. Atmos. Sci.*, **43**, 585–604.

Huang, Y.-H., M. T. Montgomery, and C.-C. Wu, 2012: Concentric eyewall formation in Typhoon Sinlaku (2008) - Part II: Axisymmetric dynamical processes. *J. Atmos. Sci.*, **69**, 662–674.

Huang, Y.-H., C.-C. Wu, and M. T. Montgomery, 2018: Concentric eyewall formation in Typhoon Sinlaku (2008). PartIII: Horizontal momentum budget analysis. *J. Atmos. Sci.*, **75**, 3541–3563.

James, I. N., 1994: *Introduction to Circulation Atmospheres*. Cambridge Atmospheric and Space Science Series. Cambridge University Press, 422 pp pp.

Kilroy, G., R. K. Smith, and M. T. Montgomery, 2016: Why do model tropical cyclones grow progressively in size and decay in intensity after reaching maturity? *J. Atmos. Sci.*, **73**, 487–503.

Marks, F. D., P. G. Black, M. T. Montgomery, and R. W. Burpee, 2008: Structure of the eye and eyewall of Hurricane Hugo (1989). *Mon. Wea. Rev.*, **136**, 1237–1259.

Montgomery, M. T., and R. K. Smith, 2017: Recent developments in the fluid dynamics of tropical cyclones. *Annu. Rev. Fluid Mech.*, **49**, 541–574.

Montgomery, M. T., J. A. Zhang, and R. K. Smith, 2014: An analysis of the observed low-level structure of rapidly intensifying and mature Hurricane Earl (2010). *Quart. Journ. Roy. Meteor. Soc.*, **140**, 2132–2146, doi:10.1002/qj.2283.

Persing, J., M. T. Montgomery, and R. K. Smith, 2025: Tropical-cyclone flow asymmetries induced by a uniform flow revisited. *Tropical Cyclone Research and Review: submitted*, **14**, 1–19.

Rogers, R., P. Reasor, and S. Lorsolo, 2013: Airborne Doppler observations of the inner-core structural differences between intensifying and steady-state tropical cyclones. *Mon. Wea. Rev.*, **141**, 2970–2991.

Rotunno, R., and G. Bryan, 2012: Effects of parameterized diffusion on simulated hurricanes. *J. Atmos. Sci*, **69**, 2284–2299.

Sampson, C. R., E. M. Fukada, J. A.Knaff, B. R. Strahl, M. J. Brennon, and T. Marchok, 2017: Tropical cyclone gale wind radii estimates for the Western North Pacific. *Weather Forecast*, **32**, 1029–1040.

Sanger, N. T., M. T. Montgomery, R. K. Smith, and M. M. Bell, 2014: An observational study of tropical-cyclone spin-up in supertyphoon Jangmi from 24 to 27 September. *Mon. Wea. Rev.*, **142**, 3–28.

Slocum, C. J., G. J. Williams, R. K. Taft, and W. H. Schubert, 2014: Tropical cyclone boundary layer shocks. *arXiv*, **1234**, 1–19.

Smith, R. K., G. Kilroy, and M. T. Montgomery, 2021a: Tropical cyclone life cycle in a three-dimensional numerical simulation. *Quart. Journ. Roy. Meteor. Soc.*, **147**, submitted.

Smith, R. K., G. Kilroy, and M. T. Montgomery, 2021b: Tropical cyclone life cycle in a three-dimensional numerical simulation. *Quart. Journ. Roy. Meteor. Soc.*, **147**, 3373–3393.

Smith, R. K., and M. T. Montgomery, 2008: Balanced depth-averaged boundary layers used in hurricane models. *Quart. Journ. Roy. Meteor. Soc.*, **134**, 1385–1395.

Smith, R. K., and M. T. Montgomery, 2010: Hurricane boundary-layer theory. *Quart. Journ. Roy. Meteor. Soc.*, **136**, 1665–1670.

Smith, R. K., and M. T. Montgomery, 2023: *Tropical cyclones: Observations and basic processes*. Elsevier, London, 411pp.

Smith, R. K., and M. T. Montgomery, 2025a: The slab boundary layer model for a translating vortex revisited. *Tropical Cyclone Research and Review*, **14**, In review.

Smith, R. K., and M. T. Montgomery, 2025b: Towards understanding the tropical cyclone lifecycle. *Tropical Cyclone Research and Review*, **14**, 119–131.

Smith, R. K., and S. Vogl, 2008: A simple model of the hurricane boundary layer revisited. *Quart. Journ. Roy. Meteor. Soc.*, **134**, 337–351.

Zhang, J. A., and M. T. Montgomery, 2012: Observational estimates of the horizontal eddy diffusivity and mixing length in the low-level region of intense hurricanes. *J. Atmos. Sci.*, **69**, 1306–1316.

Zhang, J. A., R. F. Rogers, P. D. Reasor, and J. Gamarche, 2023: The mean kinematic structure of the tropical cyclone boundary layer and its relationship to intensity change. *Mon. Wea. Rev.*, **151**, 63–84.

